Journal of Medicinal Chemistry

Article

pubs.acs.org/jmc

Exploring Selective Inhibition of the First Bromodomain of the Human Bromodomain and Extra-terminal Domain (BET) Proteins

Brigitt Raux,[†] Yuliia Voitovich,[†,‡] Carine Derviaux,[†] Adrien Lugari,[†,○] Etienne Rebuffet,[†] Sabine Milhas,[†,§] Stéphane Priet,[§] Thomas Roux,[∥] Eric Trinquet,[∥] Jean-Claude Guillemot,[§] Stefan Knapp,[⊥,¶,▽] Jean-Michel Brunel,[†] Alexey Yu. Fedorov,[‡] Yves Collette,[†] Philippe Roche,[†] Stéphane Betzi,[†] Sébastien Combes,*[,†] and Xavier Morelli*[,†]

[†]Centre National de la Recherche Scientifique (CNRS), Centre de Recherche en Cancérologie de Marseille (CRCM), UMR 7258; INSERM U1068; Institut Paoli-Calmettes; Aix-Marseille Université, UM105, 13273 Marseille, France

[‡]Department of Organic Chemistry, Lobachevsky State University of Nizhni Novgorod, Gagarina av. 23, Nizhni Novgorod 603950, Russia

[§]Screening Platform AD2P, CNRS, AFMB UMR 7257, Aix-Marseille Université, 13288 Marseille, France

[∥]Cisbio Bioassays, R&D, Parc Marcel Boiteux, BP 84175, 30200 Codolet, France

[⊥]Target Discovery Institute, University of Oxford, NDM Research Building, Roosevelt Drive, Oxford OX3 7FZ, U.K.

[¶]Structural Genomics Consortium, University of Oxford, Old Road Campus Research Building, Roosevelt Drive, Oxford OX3 7DQ, U.K.

[▽]Goethe-University, Institute for Pharmaceutical Chemistry and Buchmann Institute for Life Science, Campus Riedberg, Max-von Laue Str. 9, 60438 Frankfurt am Main, Germany

Supporting Information

ABSTRACT: A midthroughput screening follow-up program targeting the first bromodomain of the human BRD4 protein, BRD4(BD1), identified an acetylated-mimic xanthine derivative inhibitor. This compound binds with an affinity in the low micromolar range yet exerts suitable unexpected selectivity *in vitro* against the other members of the bromodomain and extra-terminal domain (BET) family. A structure-based program pinpointed a role of the ZA loop, paving the way for the development of potent and selective BET-BRD*i* probes.

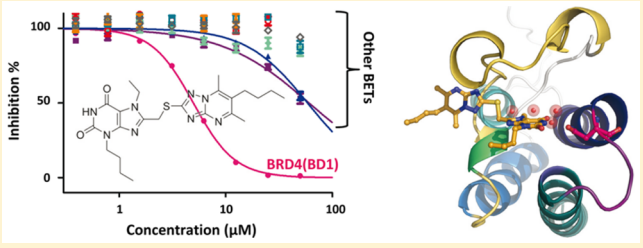

INTRODUCTION

Bromodomains (BRD) are protein interaction modules that preferentially bind ε-N-acetylated lysine residues through structurally well-defined pockets. BRDs are found in eight protein families, which include a total of 46 nuclear or cytoplasmic proteins in human with diverse structures and functions, including chromatin-modifying enzymes, helicases, chromatin remodelers, transcriptional coactivators and mediators, and the bromodomain and extra-terminal domain (BET) family of proteins.[1−3] BET proteins (BRD2, BRD3, BRD4, and the testis-specific BRDT) have a conserved modular architecture including two N-terminal tandem BRDs (BD1 and BD2). The BETs play a central role in chromatin biology by acting as tissue-specific recruitment platforms that tether complexes to acetylated histones and chromatin, facilitating the assembly of the transcriptional machinery and controlling gene expression in inflammation, viral infection, and cancer biology. For example, BRD2 is specifically recruited to acetylated histones H3 and H4, and this interaction is linked to active transcription and mitosis.[4,5] BRD2 and BRD3 are required for permissive RNA polymerase II transcription through acetylated nucleosomes,[6] and it has been suggested that BRD4 binds acetylated histones using primarily its first bromodomain (BD1).[7,8] The BD2 domain also recognizes and interacts with the acetylated region of cyclin T1, which forms a complex with the positive transcription elongation factor b and is crucial for the sustained presence of Pol II in active genes and for transcription initiation and elongation,[9] thereby regulating the expression of cell proliferation supporting genes, including c-Myc and its target genes.[10]

BET proteins are often deregulated in disease, their transcription-regulating activity being altered and thus affecting numerous growth-promoting genes and cytokines. BET proteins are known to be deregulated in cancer,[11] and the recent disclosure of pan-BET inhibitors that attenuate BRD function has allowed the validation of these drug targets, shedding light on their roles in disease. Interestingly, BRD4

Special Issue: Epigenetics

Received: November 2, 2015

DOI: 10.1021/acs.jmedchem.5b01708
J. Med. Chem. XXXX, XXX, XXX−XXX

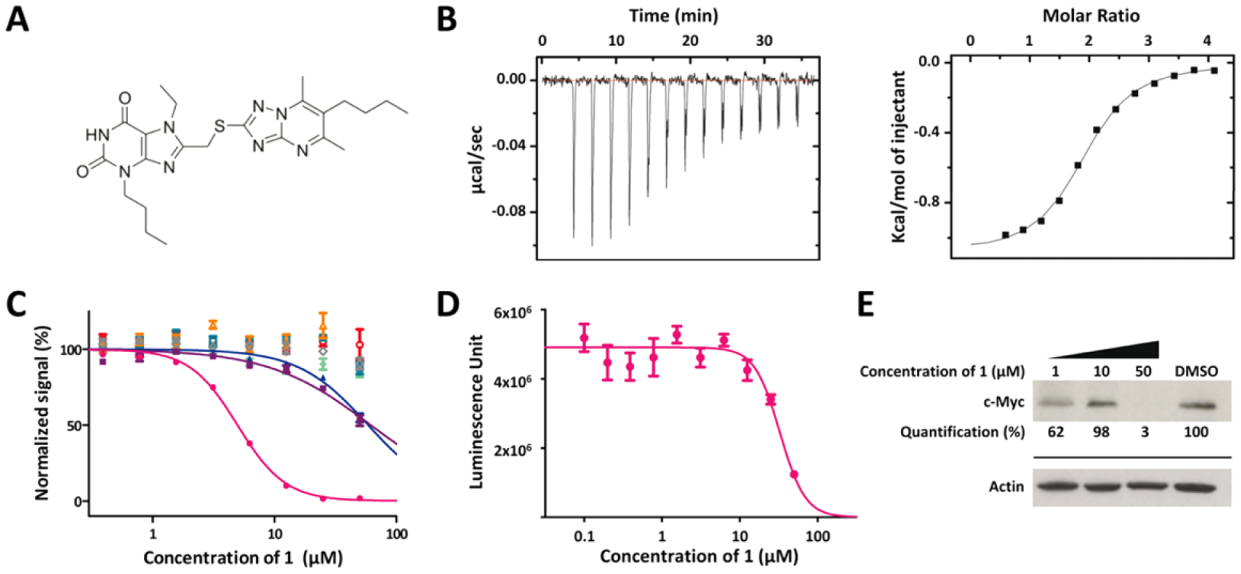

Figure 1. Identification of a selective BRD4(BD1) acetylated-mimic xanthine inhibitor **1**. (A) Structure of 3-butyl-8-(6-butyl-5,7-dimethyl-[1,2,4]triazolo[1,5-*a*]pyrimidin-2-ylsulfanylmethyl)-7-ethylxanthine, **1**. (B) Isothermal titration calorimetry (ITC) thermogram (left) and nonlinear least-squares fit model of the integrated data (right) at 35 °C (300 μM BRD4(BD1) vs 35 μM **1**) as a function of the molar ratio of ligand (cell) to the protein (syringe). (C) Homogeneous time resolved fluorescence (HTRF) selectivity assay of **1** on all BET members and ATAD2 as a non-BET control after excitation at 337 nm, energy transfer at 620 nm, and fluorescence emission at 665 nm. Fluorescence data are normalized and plotted as a function of the ligand concentration. Curves are colored by bromodomains (BRD4(BD1), pink ●; BRD3(BD1), purple ■; BRD2(BD1), blue ▲; BRDT(BD1), cyan ◆; BRD4(BD2), red ○; BRD3(BD2), gray □; BRD2(BD2), orange △; ATAD2, gray ◇). (D) Effect of **1** on Jurkat cell viability as a function of the compound concentration after 72 h incubation at 37 °C. (E) C-myc pro-oncogene downregulation profile in the presence of different concentrations of **1** at 0.5% DMSO after 24 h incubation (50 μg of loaded protein).

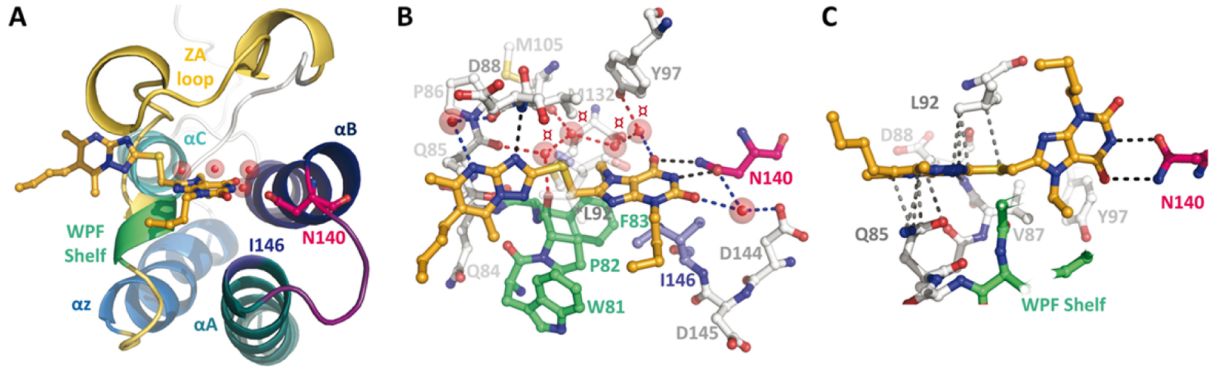

Figure 2. Molecular mode of action of **1** in the N-acetylated binding pocket of BRD4(BD1). (A) Three dimensional crystallographic structure of **1** (orange stick and ball representation) complexed with BRD4(BD1) obtained at 2.2 Å resolution (as a colored cartoon labeled by secondary structures) showing the conserved N140 residue (pink), WPF shelf (green), I146 gatekeeper residue (blue), and four highly conserved water molecules (red spheres) located at the bottom of the cavity. (B) Detailed view of **1**/BRD4(BD1) interaction. BRD4(BD1) is shown as ball and stick representation. The four conserved water molecules at the bottom of the cavity (red spheres marked with a ¤) are involved in an extensive hydrogen bond network with BRD4(BD1) (red dashed lines). Direct hydrogen bond interactions between **1** and BRD4(BD1) are shown as black dashed lines, while indirect water mediated interactions are shown as blue dashed lines. The L92 is displayed in transparency for clarity. (C) Detailed view of the van der Waals interactions (gray dashed lines) of **1** stacked between Q85 and L92 of BRD4(BD1).

occupies "superenhancers" and its inhibition leads to significant reduction of the transcript levels of only a few hundred genes,[12] in a cell-, disease-, and context-specific manner. Preclinical targeting of BETs has had initial successes, particularly in oncology. For example, in a phase I acute leukemia study, (6*S*)-4-(4-chlorophenyl)-*N*-(4-hydroxyphenyl)-2,3,9-trimethyl-6*H*-thieno[3,2-*f*][1,2,4]triazolo[4,3-*a*][1,4]diazepine-6-acetamide (OTX015),[13−16] a thienodiazepine, induced remissions, including complete remission in two patients with refractory disease, and 2-[4-(2-hydroxyethoxy)-3,5-dimethylphenyl]-5,7-dimethoxy-4(3*H*)-quinazolinone (RVX-208),[8,17] a quinazolone derivative of resveratrol that binds preferentially to the BD2 domain of BRD2 and BRD3, has already been tested in hundreds of patients in phase II clinical trials for the treatment of atherosclerosis, providing proof-of-concept that selective inhibition within the BET family is feasible. However, pan-BET inhibition might remain an issue regarding the impact on numerous transcriptional pathways and the individual tissue specific functions of BET members. The selective targeting of individual BET and the discrimination between BD1 and BD2 present one opportunity to achieve more selective transcriptional effects. Here, we follow-up on a previous midthroughput screen (MTS) using the $2P2I_{3D}$ chemical library, a structurally diverse "protein−protein interaction inhibition (2P2I)-ori-

DOI: 10.1021/acs.jmedchem.5b01708
J. Med. Chem. XXXX, XXX, XXX−XXX

Scheme 1. Synthesis of Substituted Xanthines[a]

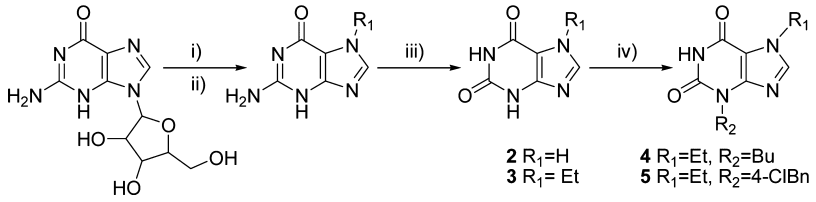

[a]Reagents and conditions: (i) EtI, DMA, 60 °C, 12 h; (ii) HCl_{aq} 3 N, reflux, 1 h, then rt NH_{3aq} 30%; (iii) $NaNO_2$, H_2O−AcOH, 50 °C, 1 h; (iv) R_2X, K_2CO_3, DMF, rt, 2 days.

ented" collection of compounds,[18−23] by focusing on a selective BRD4(BD1) acetylated-mimic xanthine inhibitor. Among the 17 hits that were identified following this screen, one xanthine derivative was found to present a low micromolar IC_{50} measured by homogeneous time-resolved fluorescence (HTRF) and an unforeseen selectivity profile among the BET family members. A structure-based investigation program around xanthine scaffold containing compounds was the starting point of this observed selectivity with a key role identified for the bromodomain ZA loop.

RESULTS AND DISCUSSION

A MTS of the $2P2I_{3D}$ chemical library against BRD4(BD1) identified 17 hits with affinities within the low micromolar range. We setup isothermal titration calorimetry (ITC) as an orthogonal assay and were able to validate direct binding for 7 out of the 17 compounds tested, with ligand efficiency (LE) values ranging from 0.20 up to 0.23. Among them, **1** (Figure 1A), a xanthine derivative, presented a K_d of 1.4 μM, driven by a large favorable entropy term ($-T\Delta S$ of −7.1 kcal/mol) as demonstrated by ITC (Figure 1B). This biophysical result suggested conformational changes and water rearrangement upon binding of the compound. Moreover, an HTRF experiment against seven out of the eight BD1 and BD2 BET domains (BRDT(BD2) was not available as single bromodomain from the company Cisbio) pinpointed a 10-fold lower IC_{50} for **1** toward BRD4(BD1) (IC_{50} of 5 μM) compared with its relative's BD1 (IC_{50} > 50 μM), and no detectable inhibition of the BD2 counterparts (Figure 1C and Table 3). In cell-based assays, **1** reduced Jurkat T cell viability in a dose-dependent manner with an EC_{50} of 27 μM. Also, **1** down-regulated c-Myc, a pro-oncogene contributing to the pathogenesis of numerous human cancers, in the same range of concentration (Figure 1D,E). We next solved the crystal structure of **1** in complex with BRD4(BD1). The cocrystal revealed the globular domain organization for BRD4(BD1)[24] and a well-defined electron density for **1** with the expected binding mode of an acetyl-lysine mimetic (Figure 2A,B and see also Supporting Information Figure S1),[25] forming the canonical hydrogen bond with the conserved asparagine N140 and a water mediated hydrogen bond with Y97 also linking the inhibitor to the conserved water network at the bottom of the binding pocket. Surprisingly, the triazolopyrimidinyl moiety stacked against the ZA channel, occupying the space at the rim of the acetyl-lysine binding site, a binding mode that has also recently been reported for benzimidazolone derivative inhibitors targeting BAZ2B bromodomain (Supporting Information Figure S2).[26−28] This triazolo moiety establishes a hydrogen bond interaction with the main chain (NH amido group) of D88, a residue conserved throughout the BET family. This interaction orientates the triazolopyrimidinyl fragment in the ZA channel, while its ring system is locked from one side by van der Waals contacts with L92 and from the other side with Q85; the pyrimidine ring sits tightly on this glutamine, which is bent by 90° to adopt this complementary orientation (Figure 2C). This BD1-conserved amino acid (except in BRDT(BD1)) is replaced by larger residues such as arginine or lysine in the BD2 subfamily (Supporting Information Figure S3). This difference could be responsible for the observed selectivity profile of **1** toward BRD4-, BRD3-, and BRD2(BD1) vs all the other BET proteins tested. Crystallographic data collection statistics are summarized in Supporting Information Table S1.

In order to gain better understanding of this selectivity profile, we undertook a structure-based program aiming to define the structure/affinity and structure/selectivity relationships by decomposing this model compound. First, the xanthine **2** and the corresponding mono- and unsymmetrically dialkylated derivatives **3**−**5** were prepared from guanosine, taking advantage of an oriented *N*7-alkylation as previously described in literature (Scheme 1).[29]

These compounds were further analyzed by HTRF, ITC, and X-ray crystallography, when available (Table 1, Figure 3).

Table 1. Effect of Various Substituted Xanthine on BRD4(BD1) Activity

	substituent		BRD4(BD1)		
compd	R_1	R_2	IC_{50}[a] (μM)	K_D[b] (μM)	LE[c]
2	H	H	*d*		*d*
3	Et	H	*d*		*d*
4	Et	Bu	13.0 ± 0.3		0.40
5	Et	4-ClBn	2.6 ± 0.1	1.8	0.37

[a]Drug concentration that inhibits protein−protein interaction by 50%. Data are the mean ± standard deviation (SD) of three experiments. [b]K_d determined by isothermal titration calorimetry. [c]Ligand Efficiency (LE) defined as the ratio of the log of the IC_{50} to the number (N) of non-hydrogen atoms of the compound LE = 1.4(-log(IC_{50})/N). [d]Not applicable.

Chemical variations of the xanthine mimicking the reference probe (6*S*)-4-(4-chlorophenyl)-2,3,9-trimethyl-6*H*-thieno[3,2-*f*][1,2,4]triazolo[4,3-*a*][1,4]diazepine-6-acetic acid 1,1-dimethylethyl ester (JQ1, PDB accession code 3MXF),[24] such as a substitution of the butyl group (compound **4**) by a chlorobenzyl one (compound **5**), allowed an optimization of the core with an IC_{50} of 2.6 μM as measured by HTRF (2-fold increased potency) and a K_d of 1.8 μM as measured by ITC. This optimized core presented a favorable enthalpy change of −6.3 kcal/mol (Figure 3A). More importantly, the selectivity profile of this optimized core **5** displayed a pan-BET inhibition profile, similarly to **4** (Figure 3B). Analysis of the cocrystal structures confirmed a characteristic recognition of the pocket

DOI: 10.1021/acs.jmedchem.5b01708
J. Med. Chem. XXXX, XXX, XXX−XXX

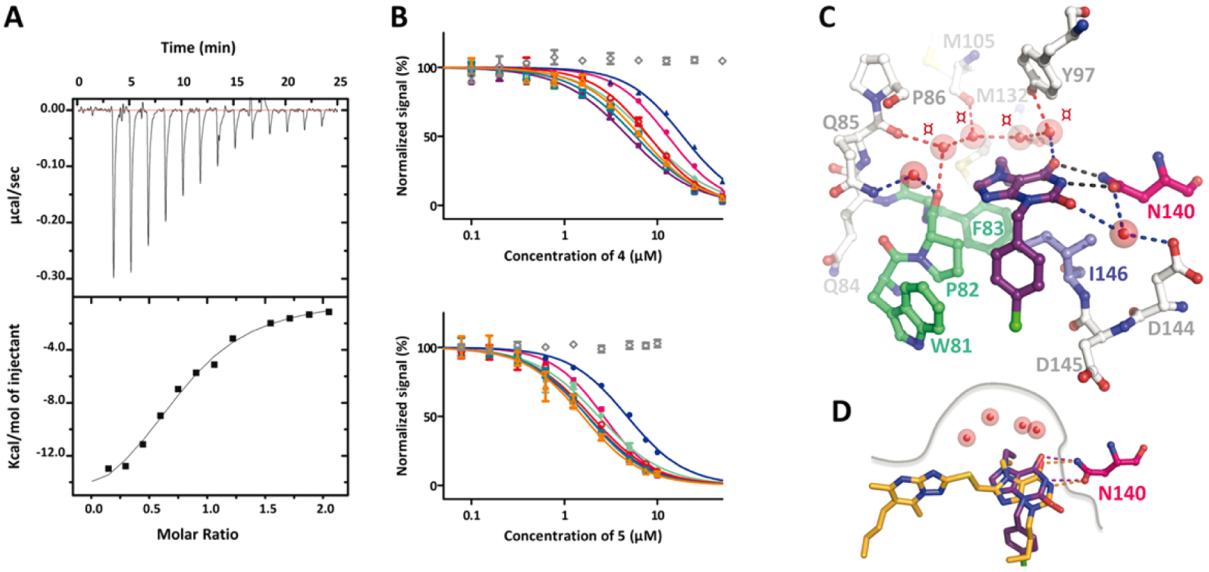

Figure 3. Studies of disubstituted xanthine derivatives as potential selective bromodomain inhibitors. (A) ITC thermogram (top) and integrated data (bottom) at 35 °C of BRD4(BD1) (100 μM in the syringe) vs **5** (10 μM in the cell) as a function of the molar ratio of ligand to protein. (B) HTRF selectivity assay of **4** (top) and **5** (bottom). The curve symbols and color scheme use the same pattern as in Figure 1. (C) Three dimensional detailed view of **5** (purple)/BRD4(BD1) molecular mode of action obtained from the crystal structure of the complex (obtained at 1.60 Å resolution) as a ball and stick representation as used for Figure 2. (D) Superimposed detailed view of the binding of **1** (orange) and **5** (purple) in the N-acetylated lysine pocket. The gray trace illustrates the cavity surface profile. Hydrogen bond interactions with the N140 are shown in orange and purple for **1** and **5**, respectively.

Scheme 2. Design and Synthesis of Triazolosulfanylmethyl-Substituted Xanthine-Based BRD4(BD1) Inhibitors 1 and 6–8[a]

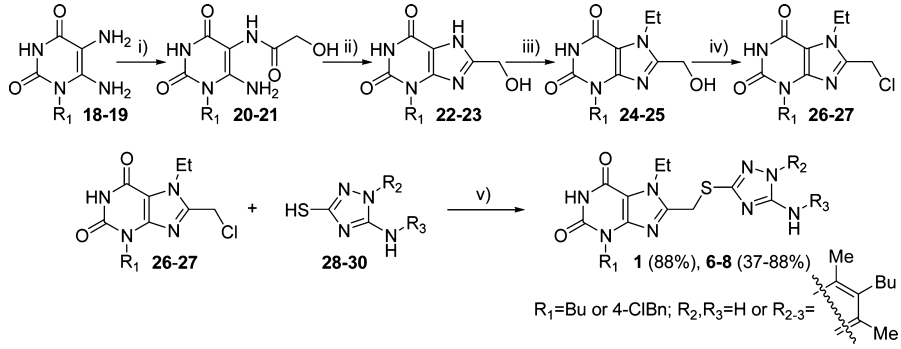

[a]Reagents and conditions: (i) glycolic acid, 120 °C, 30 min; (ii) NaOHaq., H_2O–EtOH, 85 °C, 2 h; (iii) EtI, K_2CO_3, DMF, 0 °C to rt, 12 h; (iv) $SOCl_2$, CH_2Cl_2, reflux, 15 min; (v) DIPEA, DMF, rt, 30 min.

by this core, as exemplified by the superimposition of **1** with **5** (Figure 3C,D). The core was thus not responsible (as expected) for the observed selectivity profiles of **1**.

We next questioned whether the observed selectivity profile of **1** was due to the triazolo or to the pyrimidinyl moiety of the core extension. To address this purpose, a series of *N*-3, *N*-7 disubstituted triazoloxanthine derivatives **1** and **6–8** were synthesized in ten steps following the synthetic route illustrated in Scheme 2.

The 3-alkyl-8-chloromethyl-7-ethylxanthine substrates **26** and **27** for reaction were prepared from corresponding 5,6-diaminouracils,[30] **18** and **19**, by condensation with glycolic acid followed by base induced ring closure acylation. Starting from alkylamine, the condensation with potassium cyanate afforded alkylurea **10** and **11** converted into corresponding 6-amino-uracil **14** and **15** by treating with cyanoacetic acid and sodium hydroxide successively (Supporting Information Scheme S1). Subsequent nitrosylation with sodium nitrite in aqueous acetic acid, then reduction with sodium dithionite led to expected diaminouracils **18** and **19** in good overall yields (42% and 20%, respectively).

After evaluation, compound **7** revealed an IC_{50} of 26.4 μM in HTRF, which represents a 10-fold decrease in potency compared with **5** (Tables 2 and 3). Compound **7**, however, exhibited a shift of selectivity toward BET-BD1 domains (Figure 4A and Table 3). The introduction of the triazolo fragment thus brought a decrease of potency yet drove a commencement of selectivity among BET bromodomains (BD1 vs BD2).

A potential hydrogen bond between the triazolo fragment and D88, conserved in all the BET bromodomains, could be stabilized with certain bromodomains and not with others, due to differences in the dynamics of the ZA loop, which has been demonstrated to be crucial in the binding kinetics of several BET-BRDi.[24,31,32] Superimposition of BRD4 with or without **1** illustrates structural rearrangements with displacement of the ZA loop up to 2.7 Å (Supporting Information Figure S4). These rearrangements are not observed with the "pan inhibitor"

DOI: 10.1021/acs.jmedchem.5b01708
J. Med. Chem. XXXX, XXX, XXX–XXX

Table 2. Effect of Various Triazolo-Substituted Xanthine Derivatives on BRD4(BD1) Activity

Compd	Substituent			BRD4(BD1)		
	R_1	R_2	R_3	IC_{50} (μM)[a]	K_D (μM)[b]	LE[c]
1	Bu			5.0 ± 0.1	1.4	0.22
6	4-ClBn			20.4 ± 3.6	-	0.15
7	4-ClBn	H	H	26.4 ± 0.7	-	0.17
8	Bu			> 50	-	NA

[a]Drug concentration that inhibits protein−protein interaction by 50%. Data are the mean ± standard deviation (SD) of three experiments. [b]K_d determined by isothermal titration calorimetry. [c]Ligand efficiency (LE) defined as the ratio of the IC_{50} to the number (N) of non-hydrogen atoms of the compound LE = 1.4(−log IC_{50})/N.

5, thus validating this assumption. The role of this loop and its associated variable dynamics would also explain the IC_{50} observed for **1** toward BRD4(BD1) vs BRD3(BD1) and BRD2(BD1), this hydrogen bond being more stable with BRD4(BD1). Analysis of the protein−ligand(s) interactions including hydrophobic and hydrogen-bonding contacts was carried out using LigPlot+,[33] as shown in Supporting Information Figure S5. This weak interaction prevented us from solving a nonambiguous 3D structure of **7** in complex with BRD4(BD1). However, crystals with 50% occupancy of **7** highlighted that this compound was still interacting with BRD4(BD1) and that hydrogen bond between the triazolo moiety and the main chain (NH amido group) of D88 was present, with BRD4(BD1) (Figure 4B,C). The triazolo was thus explaining only partly the observed selectivity profiles of **1**. An explanation for the selectivity profile of **1** was finally confirmed with the synthesis of **6**, the *N*-chlorobenzyl analogue of **1**. Of note, this compound was found to be less active than the original compound **1** (IC_{50} values of 20 μM vs 5 μM, respectively). However, the selectivity profile of this compound was similar to that of **1** (Figure 4A), that is, selective toward BRD4(BD1). Altogether, these data suggest that the N_3,N_7-dialkylated xanthine core (see **4** and **5**) is responsible for the pan-BET inhibition, while condensed with triazolo moiety (see **7**) it allows the preferential inhibition of BET-BD1 domains forming a hydrogen bond with the conserved D88 residue. Further condensation with pyrimidinyl moiety drives the corresponding triazolopyrimidinyl xanthine derivatives (**1** and **6**) to be selective toward BRD4(BD1) due to van der Waals interaction with the side chain of Q85. A steric clash prevents this interaction with the R54, its equivalent residue in BRDT(BD1) numbering, or the K present in the other BRDX(BD2) bromodomains. These findings suggest a potential mechanism for the selectivity of BET bromodomains. However, a more comprehensive evaluation of the role of the first bromodomain in cancer cell proliferation and chromatin biology will require the development of more selective probes with improved selectivity.

CONCLUSION

A permanent wavering in drug discovery is related to the development of pan- (multitargeted) or selective (single targeted) inhibitors. In this study, we have investigated the key structural feature responsible for the selectivity of a xanthine-based BRD4(BD1) inhibitor identified through MTS. This compound represents the first low micromolar selective inhibitor targeting BRD4(BD1) with a >10-fold ratio in binding affinity toward any other BET bromodomain tested, yet presenting low but dose−response down regulation of c-Myc levels in cell-based assay. The cocrystal structure revealed an original orientation of the triazolopyrimidinyl moiety, expanding into the ZA channel, setting the basis of a structure−selectivity relationship inside the BET family. Even though it is conserved throughout the BET family, the different dynamic behavior of the ZA loop could be exploited to tune the selectivity of BET inhibitors. Optimization of the selective BRD4(BD1) inhibitor to a probe has not been achieved yet. However, the structural features identified in this study will allow further optimization of more selective BRD4(BD1) inhibitors. The generation of such probes will allow a genuine evaluation of the biological role for each bromodomain and a validation (or not) of the interest toward the development of selective vs pan-BET inhibitors in the clinic.

EXPERIMENTAL SECTION

General Methods. All solvents were purified according to reported procedures, and the commercially available reagents were used as received. Separation by column chromatography was performed using SDS Kieselgel (70−230 mesh). Petroleum refers to the fraction with distillation range 40−65 °C. ^{1}H and ^{13}C NMR spectra were recorded using a Bruker AC400 or AC250 spectrometer. Chemical shifts, δ, are reported in ppm and coupling values, *J*, in hertz. Abbreviations for peaks are br = broad, s = singlet, d = doublet, t = triplet, q = quadruplet, quint = quintuplet, sex = sextuplet, and m = multiplet. Reaction monitoring and purity of compounds were recorded by using analytical Agilent Infinity high performance liquid

Table 3. Selectivity Profiles of Xanthine Derivatives toward BET Family Members

	IC_{50}[a] (μM)				
bromodomain	**1**	**4**	**5**	**6**[c]	**7**
BRD4(BD1)	5.0 ± 0.1	13.0 ± 0.3	2.6 ± 0.1	20.4 ± 3.6	26.4 ± 0.7
BRD3(BD1)	62.0 ± 7.8	4.8 ± 0.3	1.8 ± 1.1	*d*	31.7 ± 1.1
BRD2(BD1)	59.0 ± 2.9	18.8 ± 0.7	4.7 ± 0.1	*d*	30.0 ± 0.9
BRDT(BD1)	>100	7.9 ± 0.4	2.3 ± 0.2	*d*	>100
BRD4(BD2)	*d*	8.1 ± 0.3	1.9 ± 0.1	*d*	*d*,*e*
BRD3(BD2)	*d*	5.8 ± 0.2	1.8 ± 0.2	*d*	*d*,*e*
BRD2(BD2)	*d*	6.6 ± 0.3	1.6 ± 0.2	*d*	*d*,*e*
ATAD2[b]	>100	*d*	*d*	*d*	*d*

[a]Drug concentration that inhibits protein−protein interaction by 50%. Data are the mean ± standard deviation (SD) of three experiments. [b]ATAD2 is used as a non-BET family member bromodomain control. [c]Data above 25 μM have been excluded due to precipitation and fluorescence interference at 620 nm. [d]Not converged. [e]Fluorescence interference at 620 nm with BD2.

DOI: 10.1021/acs.jmedchem.5b01708
J. Med. Chem. XXXX, XXX, XXX−XXX

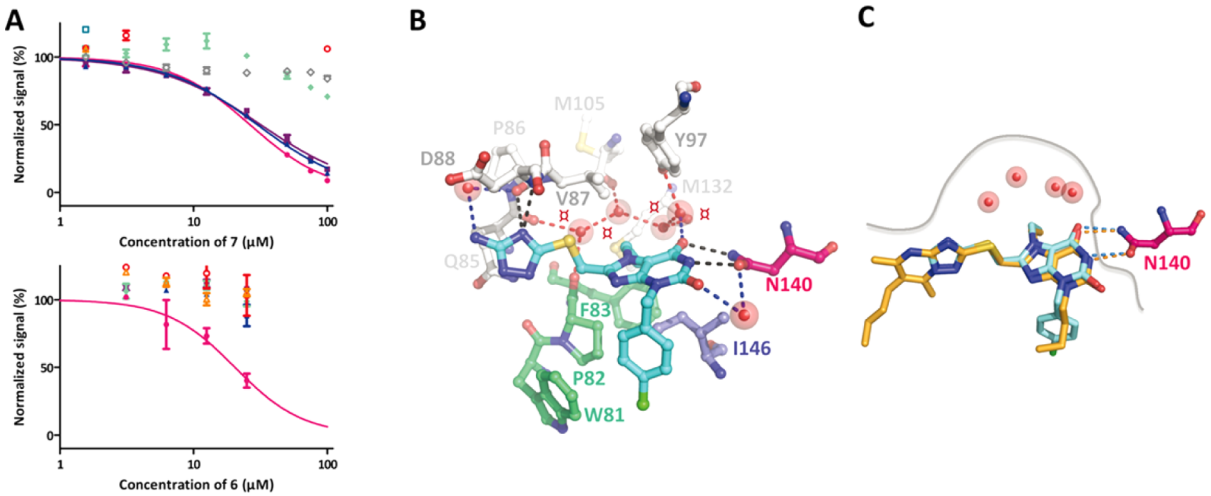

Figure 4. Structure–activity relationship of some triazolo-substituted xanthine derivatives. (A) HTRF selectivity assay results of **7** (top) and **6** (bottom). The curve symbols and color scheme use the same pattern as in Figure 1. For compound **6**, data above 25 μM have been excluded due to precipitation and fluorescence interference at 620 nm. (B) Three dimensional detailed view of **7** (cyan)/BRD4(BD1) molecular mode of action obtained from the crystal structure of the complex (1.05 Å resolution) as a ball and stick representation as used for Figure 2. (C) Superimposed detailed view of the binding of **1** (orange) and **7** (cyan) in the N-acetylated lysine pocket. Hydrogen bond interactions with the N140 are shown in orange and cyan for **1** and **7**, respectively.

chromatography (Column Zorbax SB-C18 1.8 μM (2.1 mm × 50 mm); mobile phase A 0.1% FA H_2O, B 0.1% FA MeCN, time/%B 0/10, 4/90, 7/90, 9/10, 10/10; flow rate 0.3 mL/min; diluent MeOH) with DAD at 230 nM. All tested compounds yielded data consistent with a purity of ≥95%. Low-resolution mass spectra were obtained with Agilent SQ G6120B mass spectrometer in positive electrospray mode. High-resolution mass spectra were performed at the Spectropole Analytical Laboratory of the University Paul Cezanne, Marseille.

General Procedure for the Synthesis of 8-Triazolosulfanylmethylxanthine Derivatives 1 and 6–8. To a solution of mercapto triazole derivative (0.15 mmol) in dimethylformamide (2 mL) was injected diisopropylethylamine (26 μL, 1 equiv). After 5 min under stirring, a solution of appropriate 3-alkyl-8-chloromethyl-7-ethyl-3,7-dihydro-purine-2,6-dione (1 equiv) in dimethylformamide (2 mL) was added dropwise. The resulting mixture was stirred at room temperature (30 °C) for 30 min. The solvent was distilled off under reduced pressure, and the residue was purified by column chromatography (CH_2Cl_2–MeOH) to afford the corresponding 3-alkyl-8-([1,2,4]triazolo-3-yl-sulfanylmethyl)-7-ethyl-3,7-dihydro-purine-2,6-dione.

3-Butyl-8-(6-butyl-5,7-dimethyl-[1,2,4]triazolo[1,5-a]pyrimidin-2-ylsulfanylmethyl)-7-ethyl-3,7-dihydro-purine-2,6-dione, ***1****.* Yield 88% as white solid. R_f = 0.29 (CH_2Cl_2–MeOH 10:0.5). ^{1}H NMR (250 MHz, $CDCl_3$) δ 7.88 (1H, sbroad), 4.73 (2H, s), 4.49 (2H, q, J = 7.1 Hz), 4.04 (2H,t, J = 7.4 Hz), 2.76 (3H, s), 2.73–2.69 (2H, m), 2.69 (3H, s), 1.73 (2H, quint, J = 7.4 Hz), 1.56–1.34 (6H, m), 1.40–1.28 (2H, m), 1.45 (3H, t, J = 7.4 Hz), 1.01 (3H, t, J = 7.1 Hz) and 0.95 (3H, t, J = 7.4 Hz). ^{13}C NMR (100 MHz, $CDCl_3$) δ 165.0, 164.1, 154.1, 153.8, 150.6, 150.1, 149.2, 143.5, 121.8, 42.7, 41.4, 31.9, 30.2, 28.0, 26.8, 23.8, 22.9, 20.0, 16.6, 14.0, 13.9, and 13.8. LCMS $C_{23}H_{32}N_8O_2S$ R_t = 6.755 min, m/z = 484.6, purity >99%. HRMS (ESI+) for $C_{23}H_{33}N_8O_2S$ (M + H) calcd, 485.2442; found, 485.2442.

8-(6-Butyl-5,7-dimethyl-[1,2,4]triazolo[1,5-a]pyrimidin-2-ylsulfanylmethyl)-3-(4-chlorobenzyl)-7-ethyl-3,7-dihydro-purine-2,6-dione, ***6****.* Yield 37% as light yellow solid. R_f = 0.35 (EtOAc). ^{1}H NMR (400 MHz, $CDCl_3$) δ 7.48 (2H, d, J = 8.5 Hz), 7.23 (2H, d, J = 8.5 Hz), 5.15 (2H, s), 4.71 (2H, s), 4.47 (2H, q, J = 7.2 Hz), 2.75 (3H, s), 2.73–2.70 (2H, m), 2.69 (3H, s), 1.54–1.49 (4H, m), 1.45 (3H, t, J = 7.2 Hz) and 1.00 (3H, t, J = 7.2 Hz). ^{13}C NMR (100 MHz, $CDCl_3$) δ 164.8, 164.0, 153.8, 153.7, 150.4, 149.5, 149.2, 143.4, 134.7, 133.8, 130.7, 128.6, 121.8, 107.6, 45.1, 41.3, 31.8, 27.9, 26.7, 23.7, 22.8, 16.4, 13.9, and 13.8. LCMS $C_{26}H_{29}ClN_8O_2S$ R_t = 6.728 min, m/z = 552.5, purity >99%. HRMS (ESI+) for $C_{26}H_{30}ClN_8O_2S$ (M + H) calcd, 553.1895; found, 553.1898.

8-(5-Amino-1H-[1,2,4]triazol-3-ylsulfanylmethyl)-3-(4-chlorobenzyl)-7-ethyl-3,7-dihydro-purine-2,6-dione, ***7****.* Yield 62% as yellow solid. R_f = 0.18 (EtOAc). ^{1}H NMR (250 MHz, MeOD) δ 7.38 (2H, d, J = 8.5 Hz), 7.29 (2H, d, J = 8.5 Hz), 5.12 (2H, s), 4.42 (2H, s), 4.38 (2H, q, J = 7.2 Hz), and 1.42 (3H, t, J = 7.1 Hz). ^{13}C NMR (63 MHz, MeOD) δ 156.3, 152.7, 151.5, 150.7, 136.8, 134.5, 131.1, 129.6, 108.8, 45.9, 42.2, 31.7, 16.6. LCMS $C_{17}H_{17}ClN_8O_2S$ R_t = 4.838 min, m/z = 432.5, purity >96%. HRMS (ESI+) for $C_{17}H_{18}ClN_8O_2S$ (M + H) calcd, 433.0956; found, 433.0956.

8-(5-Amino-1H-[1,2,4]triazol-3-ylsulfanylmethyl)-3-butyl-7-ethyl-3,7-dihydro-purine-2,6-dione, ***8****.* Yield 82% as light yellow powder. R_f = 0.40 (EtOAc-MeOH 6:1). ^{1}H NMR (250 MHz, DMSO-d6) δ 12.08 (1H, sbroad), 11.07 (1H, sbroad), 6.15 (2H, sbroad), 4.41 (2H, s), 4.28 (2H, q, J = 7.1 Hz), 3.85 (2H,t, J = 7.3 Hz), 1.58 (2H, quint, J = 7.3 Hz), 1.34–1.19 (5H, m) and 0.89 (3H, t, J = 7.3 Hz). ^{13}C NMR (100 MHz, DMSO-d6) δ 154.6, 150.8, 149.6, 149.1, 106.9, 41.6, 40.6, 29.9, 26.8, 19.6, 16.3, and 13.9. LCMS $C_{14}H_{20}N_8O_2S$ R_t = 4.841 min, m/z = 364.6, purity >96%. HRMS (ESI+) for $C_{14}H_{21}N_8O_2S$ (M + H) calcd, 365.1503; found, 365.1512.

■ ASSOCIATED CONTENT

Ⓢ Supporting Information

The Supporting Information is available free of charge on the ACS Publications website at DOI: 10.1021/acs.jmedchem.5b01708.

Additional figures, schemes, and tables and detailed experimental procedures for biochemistry, biology, and chemistry including spectral data and structures of synthesized compounds (PDF)

SMILES representations of compounds with associated data (CSV)

Accession Codes

PDB codes for BRD4(BD1) with bound **1**, **5** and **7**, respectively, are 5EGU, 5EIS, and 5EI4.

■ AUTHOR INFORMATION

Corresponding Authors

*S.C. E-mail: sebastien.combes@univ-amu.fr. Phone: (+33) 491-835-551.

DOI: 10.1021/acs.jmedchem.5b01708
J. Med. Chem. XXXX, XXX, XXX–XXX

*X.M. E-mail: xavier.morelli@inserm.fr. Phone: (+33)486-977-331. Mailing address: Centre de Recherche en Cancérologie de Marseille (CRCM); INSERM U1068; CNRS UMR7258; Aix-Marseille Université UM105 & Institut Paoli Calmettes, 27 Boulevard Leï Roure CS30059, 13273 Marseille Cedex 9, France.

Present Address

○A.L.: Bioaster; 40 Avenue Tony Garnier, 69007 Lyon, France.

Author Contributions

B.R. and Y.V. contributed equally to this work as first author. S.C. and X.M. contributed equally to this work as senior author.

Notes

The authors declare no competing financial interest.

■ ACKNOWLEDGMENTS

This work was supported by grants from the French Infrastructure for Integrated Structural Biology (FRISBI) ANR-10-INSB-05-01, from the "Region PACA", and from "fond FEDER" 1860-38025 CPER 2007-2013. Sabine Milhas was the recipient of a Ph.D. fellowship from Region PACA and from the "Fondation pour la Recherche Medicale" (FRM). Yuliia Voitovich was a recipient of a "Metchnikov" Ph.D. fellowship from French government. The authors acknowledge the European Synchrotron Radiation Facility for provision of synchrotron radiation facilities (under the beam time application MX1696) and thank Antoine Royant and David Flot for assistance in using beamline ID29 and ID23-2, respectively. We also thank Bruno Canard for access to facilities at UMR7257 CNRS-AMU, Marseille, and Valérie Depraetere-Ferrier for manuscript editing.

■ ABBREVIATIONS

BRD, bromodomain; BET, bromodomain and extra-terminal domain; MTS, midthroughput screening; HTRF, homogeneous time-resolved fluorescence; ITC, isothermal titration calorimetry

■ REFERENCES

(1) Filippakopoulos, P.; Knapp, S. The bromodomain interaction module. *FEBS Lett.* **2012**, *586*, 2692−2704.

(2) Filippakopoulos, P.; Picaud, S.; Mangos, M.; Keates, T.; Lambert, J.-P.; Barsyte-Lovejoy, D.; Felletar, I.; Volkmer, R.; Muller, S.; Pawson, T.; Gingras, A.-C.; Arrowsmith, C. H.; Knapp, S. Histone recognition and large-scale structural analysis of the human bromodomain family. *Cell* **2012**, *149*, 214−231.

(3) Hewings, D. S.; Rooney, T. P.; Jennings, L. E.; Hay, D. A.; Schofield, C. J.; Brennan, P. E.; Knapp, S.; Conway, S. J. Progress in the development and application of small molecule inhibitors of bromodomain-acetyl-lysine interactions. *J. Med. Chem.* **2012**, *55*, 9393−9413.

(4) Kanno, T.; Kanno, Y.; Siegel, R. M.; Jang, M. K.; Lenardo, M. J.; Ozato, K. Selective recognition of acetylated histones by bromodomain proteins visualized in living cells. *Mol. Cell* **2004**, *13*, 33−43.

(5) Huang, H.; Zhang, J.; Shen, W.; Wang, X.; Wu, J.; Wu, J.; Shi, Y. Solution structure of the second bromodomain of Brd2 and its specific interaction with acetylated histone tails. *BMC Struct. Biol.* **2007**, *7*, 57.

(6) LeRoy, G.; Rickards, B.; Flint, S. J. The double bromodomain proteins Brd2 and Brd3 couple histone acetylation to transcription. *Mol. Cell* **2008**, *30*, 51−60.

(7) Baud, M. G.; Lin-Shiao, E.; Cardote, T.; Tallant, C.; Pschibul, A.; Chan, K. H.; Zengerle, M.; Garcia, J. R.; Kwan, T. T.; Ferguson, F. M.; Ciulli, A. Chemical biology. A bump-and-hole approach to engineer controlled selectivity of BET bromodomain chemical probes. *Science* **2014**, *346*, 638−641.

(8) Picaud, S.; Wells, C.; Felletar, I.; Brotherton, D.; Martin, S.; Savitsky, P.; Diez-Dacal, B.; Philpott, M.; Bountra, C.; Lingard, H.; Fedorov, O.; Müller, S.; Brennan, P. E.; Knapp, S.; Filippakopoulos, P. RVX-208, an inhibitor of BET transcriptional regulators with selectivity for the second bromodomain. *Proc. Natl. Acad. Sci. U. S. A.* **2013**, *110*, 19754−19759.

(9) Schröder, S.; Cho, S.; Zeng, L.; Zhang, Q.; Kaehlcke, K.; Mak, L.; Lau, J.; Bisgrove, D.; Schnölzer, M.; Verdin, E.; Zhou, M.-M.; Ott, M. Two-pronged binding with bromodomain-containing protein 4 liberates positive transcription elongation factor b from inactive ribonucleoprotein complexes. *J. Biol. Chem.* **2012**, *287*, 1090−1099.

(10) Rahl, P. B.; Lin, C. Y.; Seila, A. C.; Flynn, R. A.; McCuine, S.; Burge, C. B.; Sharp, P. A.; Young, R. A. c-Myc regulates transcriptional pause release. *Cell* **2010**, *141*, 432−445.

(11) Belkina, A. C.; Denis, G. V. BET domain co-regulators in obesity, inflammation and cancer. *Nat. Rev. Cancer* **2012**, *12*, 465−477.

(12) Lovén, J.; Hoke, H. A.; Lin, C. Y.; Lau, A.; Orlando, D. A.; Vakoc, C. R.; Bradner, J. E.; Lee, T. I.; Young, R. A. Selective inhibition of tumor oncogenes by disruption of super-enhancers. *Cell* **2013**, *153*, 320−334.

(13) Boi, M.; Bonetti, P.; Ponzoni, M.; Tibiletti, M. G.; Stathis, A.; Cvitkovic, E.; Inghirami, G.; Zucca, E.; Bertoni, F. The brd-Inhibitor OTX015 shows pre-clinical activity in anaplastic large T-cell lymphoma (ALCL). *ASH Annu. Meet. Abstr., Blood* **2012**, *120*, 4872.

(14) Bonetti, P.; Boi, M.; Ponzoni, M.; Tibiletti, M. G.; Stahis, A.; Inghirami, G.; Noel, K.; Zucca, E.; Bertoni, F. *ASH Annu. Meet. Abstr., Blood* **2012**, *120*, 1657.

(15) Braun, T.; Coude, M.; Berrou, J.; Bertrand, S.; Riveiro, E.; Herait, P.; Baruchel, A.; Dombret, H.; Gardin, C. Preclinical study of the bromodomain inhibitor OTX015 in acute myeloid (AML) and lymphoid (ALL) leukemias. *ASH Annu. Meet. Abstr., Blood* **2013**, *122*, 4218.

(16) Noel, J. K.; Iwata, K.; Ooike, S.; Sugahara, K.; Nakamura, H.; Daibata, M. Development of the BET bromodomain inhibitor OTX015. *Mol. Cancer Ther.* **2013**, *12*, C244.

(17) Jahagirdar, R.; Zhang, H.; Azhar, S.; Tobin, J.; Attwell, S.; Yu, R.; Wu, J.; McLure, K. G.; Hansen, H. C.; Wagner, G. S.; Young, P. R.; Srivastava, R. A. K.; Wong, N. C. W.; Johansson, J. A novel BET bromodomain inhibitor, RVX-208, shows reduction of atherosclerosis in hyperlipidemic ApoE deficient mice. *Atherosclerosis* **2014**, *236*, 91−100.

(18) Bourgeas, R.; Basse, M.-J.; Morelli, X.; Roche, P. Atomic analysis of protein-protein interfaces with known inhibitors: the 2P2I database. *PLoS One* **2010**, *5*, e9598.

(19) Basse, M.-J.; Betzi, S.; Bourgeas, R.; Bouzidi, S.; Chetrit, B.; Hamon, V.; Morelli, X.; Roche, P. 2P2Idb: a structural database dedicated to orthosteric modulation of protein-protein interactions. *Nucleic Acids Res.* **2013**, *41*, D824−327, http://2p2idb.cnrs-mrs.fr,.

(20) Morelli, X.; Bourgeas, R.; Roche, P. Chemical and structural lessons from recent successes in protein-protein interaction inhibition (2P2I). *Curr. Opin. Chem. Biol.* **2011**, *15*, 475−481.

(21) Hamon, V.; Bourgeas, R.; Ducrot, P.; Theret, I.; Xuereb, L.; Basse, M.-J.; Brunel, J.-M.; Combes, S.; Morelli, X.; Roche, P. 2P2I HUNTER: a tool for filtering orthosteric protein-protein interac interaction modulators via a dedicated support vector machine. *J. R. Soc., Interface* **2014**, *11*, 20130860.

(22) Hamon, V.; Brunel, J. M.; Combes, S.; Basse, J.-M.; Roche, P.; Morelli, X. 2P2Ichem: focused chemical libraries dedicated to orthosteric modulation of protein-protein interactions. *MedChemComm* **2013**, *4*, 797−809.

(23) Zhang, X.; Betzi, S.; Morelli, X.; Roche, P. Focused chemical libraries–design and enrichment: an example of protein-protein interaction chemical space. *Future Med. Chem.* **2014**, *6*, 1291−1307.

(24) Filippakopoulos, P.; Qi, J.; Picaud, S.; Shen, Y.; Smith, W. B.; Fedorov, O.; Morse, E. M.; Keates, T.; Hickman, T. T.; Felletar, I.; Philpott, M.; Munro, S.; McKeown, M. R.; Wang, Y.; Christie, A. L.; West, N.; Cameron, M. J.; Schwartz, B.; Heightman, T. D.; La Thangue, N.; French, C. A.; Wiest, O.; Kung, A. L.; Knapp, S.;

DOI: 10.1021/acs.jmedchem.5b01708
J. Med. Chem. XXXX, XXX, XXX−XXX

Bradner, J. E. Selective inhibition of BET bromodomains. *Nature* **2010**, *468*, 1067−1073.
(25) Vollmuth, F.; Blankenfeldt, W.; Geyer, M. Structures of the dual bromodomains of the P-TEFb-activating protein Brd4 at atomic resolution. *J. Biol. Chem.* **2009**, *284*, 36547−36556.
(26) Drouin, L.; McGrath, S.; Vidler, L. R.; Chaikuad, A.; Monteiro, O.; Tallant, C.; Philpott, M.; Rogers, C.; Fedorov, O.; Liu, M.; Akhtar, W.; Hayes, A.; Raynaud, F.; Müller, S.; Knapp, S.; Hoelder, S. Structure enabled design of BAZ2-ICR, a chemical probe targeting the bromodomains of BAZ2A and BAZ2B. *J. Med. Chem.* **2015**, *58*, 2553−2559.
(27) Bennett, J.; Fedorov, O.; Tallant, C.; Monteiro, O.; Meier, J.; Gamble, V.; Savitsky, P.; Nunez-Alonso, G. A.; Haendler, B.; Rogers, C.; Brennan, P. E.; Müller, S.; Knapp, S. Discovery of a chemical tool inhibitor targeting the bromodomains of TRIM24 and BRPF. *J. Med. Chem.* **2015**, DOI: 10.1021/acs.jmedchem.5b00458.
(28) Palmer, W. S.; Poncet-Montange, G.; Liu, G.; Petrocchi, A.; Reyna, N.; Subramanian, G.; Theroff, J.; Yau, A.; Kost-Alimova, M.; Bardenhagen, J. P.; Leo, E.; Shepard, H. E.; Tieu, T. N.; Shi, X.; Zhan, Y.; Zhao, S.; Barton, M. C.; Draetta, G.; Toniatti, C.; Jones, P.; Geck Do, M.; Andersen, J. N. Structure-guided design of IACS-9571, a selective high-affinity dual TRIM24-BRPF1 bromodomain inhibitor. *J. Med. Chem.* **2015**, DOI: 10.1021/acs.jmedchem.5b00405.
(29) Vidal, A.; Giraud, I.; Madelmont, J.-C. Improved synthesis of 7-(alkyl/aryl)guanine. *Synth. Commun.* **2004**, *34*, 3359−3365.
(30) Kalla, R. V.; Elzein, E.; Perry, T.; Li, X.; Gimbel, A.; Yang, M.; Zeng, D.; Zablocki, J. Selective, high affinity A2B adenosine receptor antagonists: N-1 monosubstituted 8-(pyrazol-4-yl)xanthines. *Bioorg. Med. Chem. Lett.* **2008**, *18*, 1397−1401.
(31) Kuang, M.; Zhou, J.; Wang, L.; Liu, Z.; Guo, J.; Wu, R. Binding Kinetics versus Affinities in BRD4 Inhibition. *J. Chem. Inf. Model.* **2015**, *55*, 1926−1935.
(32) Ran, T.; Zhang, Z.; Liu, K.; Lu, Y.; Li, H.; Xu, J.; Xiong, X.; Zhang, Y.; Xu, A.; Lu, S.; Liu, H.; Lu, T.; Chen, Y. Insight into the key interactions of bromodomain inhibitors based on molecular docking, interaction fingerprinting, molecular dynamics and binding free energy calculation. *Mol. BioSyst.* **2015**, *11*, 1295−1304.
(33) Laskowski, R. A.; Swindells, M. B. LigPlot+: multiple ligand-protein interaction diagrams for drug discovery. *J. Chem. Inf. Model.* **2011**, *51*, 2778−2786.

DOI: 10.1021/acs.jmedchem.5b01708
J. Med. Chem. XXXX, XXX, XXX−XXX